Waveform control of terahertz light via electron beam longitudinal phase-space manipulation

Yifan Liang,[1] Xiaofan Wang,[1,*] Tong Li,[2] Jitao Sun,[1] Zhuoyuan Liu,[2] Jiayue Yang,[3] Yong Yu,[1] Qili Tian,[2] Zhigang He,[3] Hongfei Wang,[1] Li Zeng,[1] Hao Sun,[1] Qinghao Zhu,[1] Xuan Liu,[1] Guorong Wu,[3,†] Weiqing Zhang,[3,‡] Xueming Yang,[3] Chuanxiang Tang,[2] and Lixin Yan[2,§]

[1]*Institute of Advanced Light Source Facilities, Shenzhen 518107, China*

[2]*Department of Engineering Physics, Tsinghua University, Beijing 100084, China*

[3]*Dalian Coherent Light Source and State Key Laboratory of Chemical Reaction Dynamics, Dalian Institute of Chemical Physics, Chinese Academy of Sciences, Dalian 116023, China*

(Received 26 November 2025; accepted 11 April 2026; published 4 May 2026)

Synthesizing intense terahertz (THz) waveforms with user-defined electric field profiles represents a pivotal challenge for controlling matter at ultrafast timescales. While relativistic electron beams can serve as a versatile source of coherent radiation, conventional schemes lack the ability to deterministically sculpt the temporal structure of the emitted light. Here, we experimentally demonstrate a paradigm for generating tailored THz waveforms by manipulating the longitudinal phase space of the electron beam. By controlling the nonlinear longitudinal correlation of an energy-chirped electron beam, we generate a microbunch train with a chirped density modulation. When coupled to a tapered undulator, this structured beam produces coherent radiation, whose spectral-temporal properties are tunable via adjustment of the undulator taper. Autocorrelation measurements confirm the emission of chirped pulses spanning 8–13 THz, with spectral characteristics that align with simulations of the beam structure. Our approach, establishing a direct link between beam dynamics and light-field synthesis, opens a pathway toward customizable high-field waveforms for advanced coherent control experiments.

DOI: 10.1103/xw7z-5c2d

I. INTRODUCTION

The terahertz (THz) spectral regime, bridging the gap between electronics and photonics, unlocks possibilities for probing matter and controlling quantum systems [1–8]. To fully harness these transformative opportunities, a critical technological advancement is imperative: the creation of advanced radiation sources capable of delivering not only high-field, ultrafast terahertz pulses with multimegavolt-per-centimeter field strengths and femtosecond-scale duration, but also precisely tailored electromagnetic field profiles with user-definable temporal and spectral characteristics. This dual capability represents a fundamental prerequisite for unlocking sophisticated coherent control applications that demand customized light-matter interactions beyond what conventional single-cycle pulses can provide. While laser-based sources like optical rectification can produce powerful single-cycle pulses [9–11], their temporal structure is largely dictated by the intrinsic properties of the laser and the nonlinear crystal.

In parallel, accelerator-based sources, particularly those employing prebunched electron beams, offer a powerful alternative for generating intense coherent radiation from microwaves to x-rays [12–20]. The fundamental principle involves imprinting a periodic density modulation on a relativistic electron beam (microbunching), which then radiates coherently upon passing through a magnetic undulator. Significant progress has been made in generating such microbunching at THz frequencies [21–32], for instance, by leveraging longitudinal space-charge oscillations [25,28,32]. However, the primary focus of these studies has overwhelmingly been on enhancing the intensity of the radiation, often aiming for a narrow-band spectrum or a simple, short pulse, leaving the more ambitious goal of deterministic THz waveform synthesis largely unexplored.

The synthesis of complex, multicycle waveforms requires moving beyond uniform microbunching. It demands the generation of a chirped density modulation—a microbunch train where the spacing between microbunches varies along the electron beam. Such a structure, when radiating, naturally produces a frequency-swept electromagnetic wave. The emitted fields from successive microbunches can constructively or destructively interfere [33–36], and by controlling the chirp rate, one can in principle sculpt the temporal profile of the resulting THz pulse. The central scientific challenge, therefore, is to develop a robust method to encode a desired temporal

*Contact author: wangxf@mail.iasf.ac.cn
†Contact author: wugr@dicp.ac.cn
‡Contact author: weiqingzhang@dicp.ac.cn
§Contact author: yanlx@mail.tsinghua.edu.cn

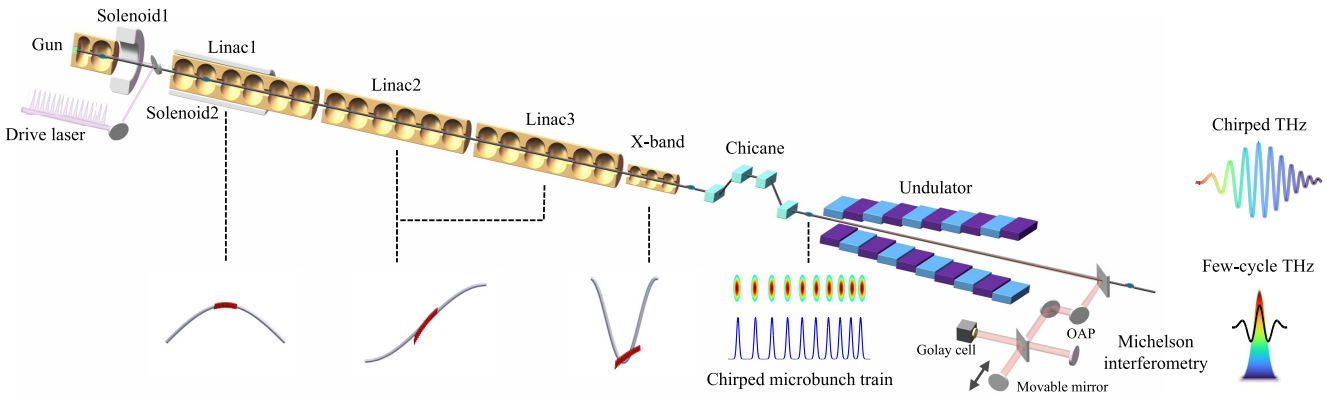

FIG. 1. Schematic layout of the beamline for chirped electron microbunch train generation. OAP: off-axis parabolic mirror.

structure directly into the electron beam's longitudinal phase space and to demonstrate its translation into a tailored light field.

In this article, we report the experimental demonstration of tailored THz waveform generation through deterministic electron beam longitudinal phase-space manipulation. We introduce a method to generate a chirped electron microbunch train by combining space charge effects, a nonlinear energy chirp imparted by off-crest radio-frequency (rf) acceleration, and a magnetic chicane for compression. We demonstrate that the chirp rate of the microbunching can be actively controlled, effectively sculpting the electron beam to serve as a structured radiation source. When this sculpted beam interacts with a tapered undulator, the spectral properties of the emitted coherent radiation are shown to be tunable, providing direct evidence of the encoded chirp. Crucially, by comparing the measured radiation spectra with simulations, we verify that the synthesized THz pulse duration can be compressed into the single-cycle regime. Our work establishes a direct link between engineered beam dynamics and tailored light-field generation, opening a pathway toward fully customizable photon sources for probing and controlling matter at ultrafast timescales.

II. EXPERIMENTAL SETUP AND RESULTS

The experiment was conducted at Dalian Coherent Light Source [37], with the schematic layout shown in Fig. 1. An electron beam with a total charge of 700 pC, generated by an (rf) photocathode gun, was initially density modulated by a laser pulse train with a period of $\lambda = 150$ μm. The beam transport system comprised three S-band linear accelerators (linacs), with focusing provided by two solenoids: one positioned at the gun exit and another along the first linac. The first linac was set at the rf crest for maximum acceleration, boosting the beam energy to around 51 MeV. Subsequent beam manipulation was accomplished by operating the second and third linacs off crest to introduce a negative energy chirp, with the beam head having lower energy than the beam tail. The peak electric fields in these linacs were finely adjusted to regulate both the chirp amplitude and longitudinal compression dynamics. To control the shape of the longitudinal phase space, an X-band, fourth-harmonic rf cavity was employed prior to the compression stage. The beam then traversed a magnetic chicane whose dispersion properties facilitated bunch compression. Finally, the conditioned beam was delivered to a planar undulator comprising 20 periods with a 5 cm period length for radiation generation. A THz radiation measurement platform was installed right after the undulator exit. The emitted THz pulses were reflected by an aluminum-coated mirror to exit the vacuum chamber and were subsequently directed into a Michelson interferometer for autocorrelation measurements.

When the electron beam generated in the rf photocathode gun carries a strong initial density modulation (with a period of λ), nonlinear longitudinal space-charge oscillations arise. These oscillations produce higher harmonics of λ, leading to sharp current spikes in the longitudinal charge distribution. The beam's longitudinal distribution becomes fixed upon acceleration to tens of MeV energy levels, with current spike structures being preserved throughout subsequent drift transport due to negligible longitudinal dispersion effects in the beam dynamics. These current spikes subsequently generate intense longitudinal space-charge fields that imprint significant energy modulations along the bunch. When coupled with a longitudinal energy chirp, the time-of-flight difference in the magnetic chicane induces compression. In nonlinear compression regimes characterized by higher-order energy chirp components and second-order dispersion terms in the chicane optics, the compression rate becomes position dependent. This results in stronger compression at the beam head (higher chirp rate due to the rf field) compared to the tail, leading to a longitudinally varying microbunch spacing. The microbunch spacing chirp rate can be tuned by shaping the energy chirp nonlinearity via the X-band harmonic cavity that modifies the longitudinal phase space.

To systematically analyze the longitudinal beam dynamics throughout the acceleration and compression process, we performed start-to-end numerical simulations using the particle-tracking code ASTRA [38], with full three-dimensional space-charge effects incorporated. Figure 2 illustrates the beam longitudinal phase space under different phase conditions ($\varphi = -180°$, $-170°$, and $-160°$) of the X-band cavity, which controls the nonlinearity of the energy chirp. The

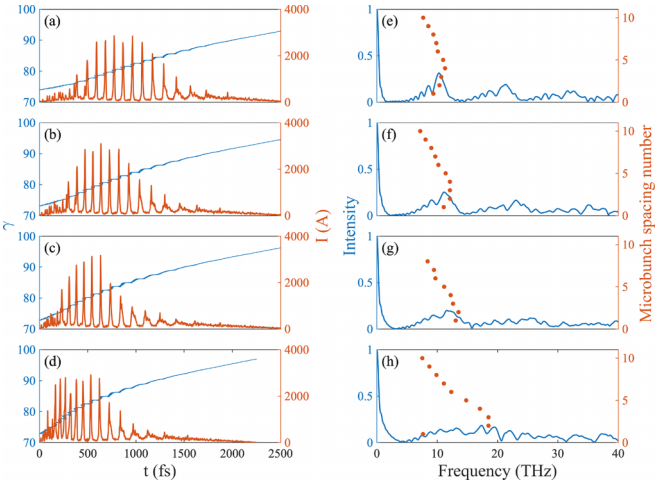

FIG. 2. (a)–(d) Simulated beam longitudinal phase-space and current distribution under different X-band cavity phase settings. The beam head is to the left. (e)–(h) Corresponding Fourier transforms and extracted microbunch spacing. (a), (e) $\varphi = -180^\circ$, $R_{56} = -7.7$ mm; (b), (f) $\varphi = -170^\circ$, $R_{56} = -6.7$ mm; (c), (g) $\varphi = -160^\circ$, $R_{56} = -5.9$ mm; (d), (h) $\varphi = -160^\circ$, $R_{56} = -6.3$ mm.

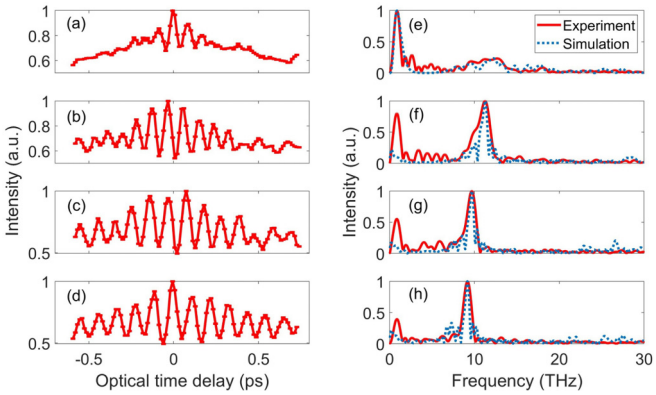

FIG. 3. (a)–(d) Autocorrelation measurements and (e)–(h) their corresponding Fourier transforms. (a), (e) Undulator parameter $K = 2.48$; (b), (f) $K = 3.25$; (c), (g) $K = 3.64$; (d), (h) $K = 3.8$.

cavity voltage is fixed at ∼10 MV. As can be seen in Figs. 2(a)–2(d), the longitudinal phase-space distributions exhibit distinct compression dynamics, where $\varphi = -180^\circ$ [Fig. 2(a)] corresponds to optimal second-order phase-space correction, while $\varphi = -170^\circ$ [Fig. 2(b)] and $\varphi = -160^\circ$ [Figs. 2(c) and 2(d)] introduce moderate and significant second-order correlations, respectively. These correlations cause the higher-chirp-rate beam head to compress faster than the lower-chirp-rate beam tail, reducing the microbunch spacing from the tail to the head.

Fourier analysis of the microbunching structures, as depicted in Figs. 2(e)–2(h), reveals significant variations in spectral distributions. While the $\varphi = -180^\circ$ case [Figs. 2(a) and 2(e)] produces a narrow-band spectrum, the $\varphi = -160^\circ$ configuration produces strong nonlinearities manifested as nonuniform microbunch spacings and broadband frequency components. The enhanced dispersion setting in Fig. 2(d), achieved by increasing the magnetic chicane strength relative to Fig. 2(c), further compresses the electron beam and significantly modifies the microbunching spectrum, extending the frequencies to 7–18 THz range.

The experimental validation of the generation of chirped microbunching is provided by the THz spectra measured under different undulator configurations. In the experiment, we set the X-band cavity voltage at 10 MV and the phase at approximately -160°. The undulator magnetic field strength B_0 was modified through gap adjustments to satisfy the fundamental resonance condition

$$\lambda_r = \frac{\lambda_u}{2\gamma^2}\left(1 + \frac{K^2}{2}\right), \tag{1}$$

where λ_r is the resonant radiation wavelength, $\lambda_u = 5$ cm denotes the undulator period length, γ is the relativistic Lorentz factor, and $K = \frac{eB_0\lambda_u}{2\pi m_e c}$ represents the dimensionless undulator parameter. Here, e, m_e, and c denote the electron charge, electron rest mass, and speed of light in vacuum, respectively.

Figure 3 presents the measured autocorrelation traces [Figs. 3(a)–3(d)] together with their corresponding spectral distributions and the simulated spectra [Figs. 3(e)–3(h)]. The autocorrelation length of our measurements is 0.4 mm, which corresponds to a spectral resolution of 0.75 THz. While the detailed atmospheric absorption peaks are beyond the resolving capability of our setup, and the correction for the in-air spectrometer transmittance presents nontrivial challenges, these limitations do not compromise the validity of the spectral diagnosis. To avoid atmospheric absorption in future user experiments, all optical transport and diagnostic components will be housed in a vacuum chamber.

The simulated spectra were obtained using the expression $I(\omega) \propto W_1(\omega)b^2(\omega)g^2(\omega)$, where $W_1(\omega)$ is the single-electron coherent synchrotron radiation (CSR) spectrum calculated with the code SPECTRA [39], $b(\omega)$ is the bunching factor simulated with ASTRA, and $g(\omega) = 1 - e^{-\xi^2\omega^2}$ is an analytical filter function introduced to account for the stronger diffraction effects affecting the low-frequency components [40,41]. The design of this filter is physically motivated by the far-field aperturing of a diffraction-limited transverse Gaussian-mode photon beam, a scenario that aligns with the experimental setup in the present measurement. The chosen cutoff frequency ξ^{-1} is 0.8 THz, which allows the simulated spectral intensity to match the low-frequency peak observed in the measured spectrum.

The characteristic low-frequency spectral features observed at ∼1 THz across all experimental configurations in Fig. 3 originate from collective radiation effects of the picosecond-scale bunch envelope, whereas the higher-frequency peaks correspond to microbunch-induced coherent emission. When the undulator gap is set to 20 mm ($K = 2.48$), the undulator resonant frequency (∼19 THz) is mismatched relative to the microbunching frequency, and no resonant spectral components are observed. Under this condition, the emission is primarily due to CSR from the undulator and coherent transition radiation (CTR) from the downstream mirror—both reflecting the spectral characteristics of the electron microbunch train. Given that the measured CSR signal exceeds the CTR signal by a factor of ∼10, we consider only CSR in our quantitative analysis. Spectral

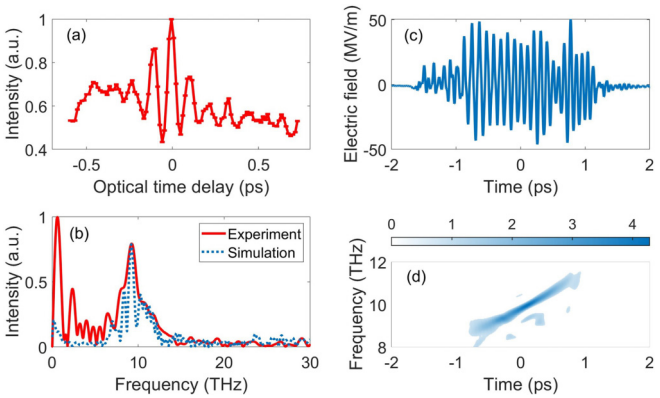

FIG. 4. Measurements and simulation results with a linear undulator taper from $K = 3.88$ to $K = 3.25$. (a) Autocorrelation measurements. (b) Spectrum from the autocorrelation measurements and the simulation. (c) Temporal distribution of the simulated electric field. (d) Time-frequency representation of the simulated electric field.

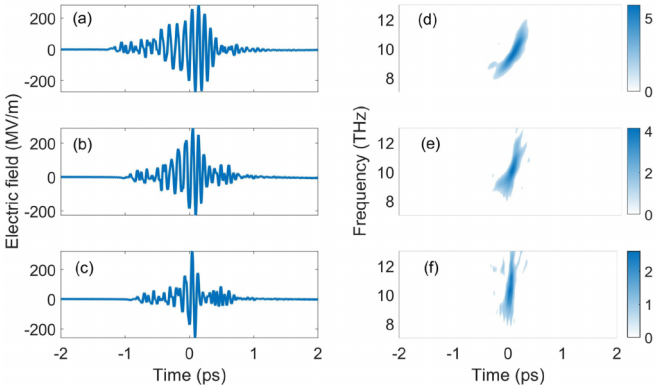

FIG. 5. (a)–(c) Simulated electric fields of the emitted radiation and (d)–(f) their corresponding time-frequency representations. (a), (d) Tapering parameter $\alpha = 0.5\ \mathrm{m}^{-1}$; (b), (e) $\alpha = 1\ \mathrm{m}^{-1}$; (c), (f) $\alpha = 1.4\ \mathrm{m}^{-1}$. The electron beam has the longitudinal distribution shown in Fig. 2(c), and the undulator has ten periods and the undulator parameter K at the undulator entrance is 3.97.

analysis of Fig. 3(e) reveals broadband emission spanning 8–13 THz. The agreement between the measured broadband spectrum and the simulated spectrum in Fig. 3(e) strongly indicates a chirped microbunching structure, characterized by a reduction in bunch spacing from approximately 125 to 77 fs. The minor discrepancies may due to the nonideal experimental conditions and the frequency resolution (0.75 THz) of our measurement setup.

By adjusting the undulator parameter K from 3.8 to 3.25 through gap changes [uniform undulator, Figs. 3(b)–3(d)], we achieved tuning of the central radiation frequency from 9.17 to 11.26 THz, corresponding to resonant energies decreasing from 40 MeV to 38.7 MeV according to the undulator resonance condition in Eq. (1). Given the measured negative energy chirp of the beam (i.e., the bunch head had lower energy than the tail), our analysis shows that the central frequency is inversely proportional to the beam energy. This result directly supports the simulation prediction of stronger longitudinal compression at the beam head, thereby confirming the key dynamical feature in the bunch.

When the chirped electron microbunch train traverses a tapered undulator, the resulting radiation pulse duration can be actively controlled through finely engineered destructive interference between successive radiation fields. This interference effect arises from the combined phase shift induced by the intrinsic microbunch spacing chirp and the undulator taper-induced tuning, enabling continuous adjustment of the synthesized pulse duration. The undulator utilized in our experiment can provide a linear longitudinal taper, with its magnetic field profile described by

$$B(z) = B_0(1 - \alpha z), \tag{2}$$

where B_0 represents the peak magnetic field amplitude at the undulator entrance ($z = 0\,\mathrm{m}$) and α is the tapering parameter. Operating the undulator at its peak field amplitude of 0.83 T with a tapering parameter $\alpha \approx 0.16\,\mathrm{m}^{-1}$ (the maximum achievable tapering for our undulator), as evident from Figs. 4(a) and 4(b), we observed that the autocorrelation measurements exhibit fewer cycles accompanied by spectral broadening. Figures 4(c) and 4(d) present the simulated temporal electric field distribution and the corresponding time-frequency representation, respectively. The latter reveals a clearly discernible chirp structure

To verify the mechanism of phase-based coherent synthesis, we present systematic numerical evidence in Fig. 5. The spectral amplitude resulting from a chirped microbunch train and a tapered undulator can be expressed as $I(\omega) = A_0 e^{i(\alpha_1-\alpha_2)(\omega-\omega_0)^2}$, where α_1 depends on the chirped microbunch train and α_2 is determined by the tapered undulator [33,34]. If the microbunch spacing is uniform ($\alpha_1 = 0$), the chirp rate of the emitted THz spectrum is determined by the undulator tapering α_2 and the generated pulse is inherently multicycle. In the simulations, the same chirped microbunch train is employed to maintain α_1 nonzero and constant, while the undulator tapering rate is increased to gradually enhance α_2. As shown in Fig. 5, increasing α_2 causes the temporal localization of different frequency components to narrow. When $\alpha_1 = \alpha_2$, the temporal electric field evolves into a quasi-single-cycle pulse. The physical origin of this compression is phase-based coherent synthesis: The undulator taper introduces an additional phase shift that compensates the intrinsic chirp of the electron beam. This allows constructive and destructive interference of radiation emitted from different longitudinal positions, effectively compressing the pulse envelope.

III. CONCLUSION

In summary, we have demonstrated a paradigm for THz waveform control leveraging the electron beam as a dynamically configurable radiation source. The central achievement lies in demonstrating a direct and deterministic relationship between an engineered beam property, specifically, a chirped density modulation, and the resulting THz waveform, characterized by its tailored spectral and temporal structure. Active control over the output radiation was conclusively verified through systematic undulator tuning, which selectively coupled distinct segments of the structured electron beam to

emission at different frequencies. The underlying principles of phase-space engineering and undulator-based pulse shaping exhibit broad applicability beyond the THz domain. This framework can be extended to shorter wavelengths, offering a scalable pathway toward fully customizable photon sources across the electromagnetic spectrum, from infrared to x-ray free-electron lasers.

ACKNOWLEDGMENTS

We thank the Dalian Coherent Light Source [42] for excellent support during the experiments. We would also like to thank Yin Kang, Yue Wang, Wei Wang, Wei Wei, Likai Wang, Ming Liu, Liuping Chen, Guoqing Zhang, Lei He, Chunguang Wang, Feng Zhao, Jianping Wei, Zhijun Qi, and Wenjie Cheng for technical support. This work was supported by the National Natural Science Foundation of China (Grants No. 12305153, No. 11835004, No. 22288201, and No. 124B2104), LiaoNing Revitalization Talents Program (No. XLYC2202030), Beijing Outstanding Young Scientist Program (No. JWZQ20240101006), the Strategic Priority Research Program of the Chinese Academy of Sciences (No. XDB0970000, Subject No. XDB0970100), the Scientific Instrument Developing Project of Chinese Academy of Sciences (Grant No. GJJSTD20220001), and the High Performance Computing Center, Tsinghua University.

DATA AVAILABILITY

The data that support the findings of this article are not publicly available. The data are available from the authors upon reasonable request.

[1] S. Baierl, M. Hohenleutner, T. Kampfrath, A. K. Zvezdin, A. V. Kimel, R. Huber, and R. V. Mikhaylovskiy, Nonlinear spin control by terahertz-driven anisotropy fields, Nat. Photon. **10**, 715 (2016).

[2] T. L. Cocker, D. Peller, P. Yu, J. Repp, and R. Huber, Tracking the ultrafast motion of a single molecule by femtosecond orbital imaging, Nature (London) **539**, 263 (2016).

[3] V. Jelic, K. Iwaszczuk, P. H. Nguyen, C. Rathje, G. J. Hornig, H. M. Sharum, J. R. Hoffman, M. R. Freeman, and F. A. Hegmann, Ultrafast terahertz control of extreme tunnel currents through single atoms on a silicon surface, Nat. Phys. **13**, 591 (2017).

[4] S. Schlauderer, C. Lange, S. Baierl, T. Ebnet, C. P. Schmid, D. C. Valovcin, A. K. Zvezdin, A. V. Kimel, R. V. Mikhaylovskiy, and R. Huber, Temporal and spectral fingerprints of ultrafast all-coherent spin switching, Nature (London) **569**, 383 (2019).

[5] L. Luo, X. Yang, X. Liu, Z. Liu, C. Vaswani, D. Cheng, M. Mootz, X. Zhao, Y. Yao, C. Z. Wang, K. M. Ho, I. E. Perakis, M. Dobrowolska, J. K. Furdyna, and J. Wang, Ultrafast manipulation of topologically enhanced surface transport driven by mid-infrared and terahertz pulses in Bi_2Se_3, Nat. Commun. **10**, 607 (2019).

[6] E. A. Mashkovich, K. A. Grishunin, R. M. Dubrovin, A. K. Zvezdin, R. V. Pisarev, and A. V. Kimel, Terahertz light–driven coupling of antiferromagnetic spins to lattice, Science **374**, 1608 (2021).

[7] M. Basini, M. Pancaldi, B. Wehinger, M. Udina, V. Unikandanunni, T. Tadano, M. C. Hoffmann, A. V. Balatsky, and S. Bonetti, Terahertz electric-field-driven dynamical multiferroicity in $SrTiO_3$, Nature (London) **628**, 534 (2024).

[8] Z. Zhang, F. Y. Gao, Y.-C. Chien, Z.-J. Liu, J. B. Curtis, E. R. Sung, X. Ma, W. Ren, S. Cao, P. Narang, A. von Hoegen, E. Baldini, and K. A. Nelson, Terahertz-field-driven magnon upconversion in an antiferromagnet, Nat. Phys. **20**, 788 (2024).

[9] J. A. Fülöp, S. Tzortzakis, and T. Kampfrath, Laser-driven strong-field terahertz sources, Adv. Opt. Mater. **8**, 1900681 (2020).

[10] X. Wu, D. Kong, S. Hao, Y. Zeng, X. Yu, B. Zhang, M. Dai, S. Liu, J. Wang, Z. Ren, *et al.*, Generation of 13.9-mJ terahertz radiation from lithium niobate materials, Adv. Mater. **35**, 2208947 (2023).

[11] X. Zhu, D. R. Bacon, J. Madéo, and K. M. Dani, High field single- to few-cycle THz generation with lithium niobate, Photonics **8**, 183 (2021).

[12] L.-H. Yu, M. Babzien, I. Ben-Zvi, L. F. DiMauro, A. Doyuran, W. Graves, E. Johnson, S. Krinsky, R. Malone, I. Pogorelsky, *et al.*, High-gain harmonic-generation free-electron laser, Science **289**, 932 (2000).

[13] S. E. Korbly, A. S. Kesar, J. R. Sirigiri, and R. J. Temkin, Observation of frequency-locked coherent terahertz Smith-Purcell radiation, Phys. Rev. Lett. **94**, 054803 (2005).

[14] E. Hemsing, M. Dunning, B. Garcia, C. Hast, T. Raubenheimer, G. Stupakov, and D. Xiang, Echo-enabled harmonics up to the 75th order from precisely tailored electron beams, Nat. Photon. **10**, 512 (2016).

[15] Y. Ding, K. L. F. Bane, W. Colocho, F.-J. Decker, P. Emma, J. Frisch, M. W. Guetg, Z. Huang, R. Iverson, J. Krzywinski, H. Loos, A. Lutman, T. J. Maxwell, H.-D. Nuhn, D. Ratner, J. Turner, J. Welch, and F. Zhou, Beam shaping to improve the free-electron laser performance at the Linac Coherent Light Source, Phys. Rev. Accel. Beams **19**, 100703 (2016).

[16] S. Huang, Y. Ding, Y. Feng, E. Hemsing, Z. Huang, J. Krzywinski, A. A. Lutman, A. Marinelli, T. J. Maxwell, and D. Zhu, Generating single-spike hard x-ray pulses with nonlinear bunch compression in free-electron lasers, Phys. Rev. Lett. **119**, 154801 (2017).

[17] C. Feng and H. Deng, Review of fully coherent free-electron lasers, Nucl. Sci. Tech. **29**, 160 (2018).

[18] P. Franz, S. Li, T. Driver, R. R. Robles, D. Cesar, E. Isele, Z. Guo, J. Wang, J. P. Duris, K. Larsen, *et al.*, Terawatt-scale attosecond X-ray pulses from a cascaded superradiant free-electron laser, Nat. Photon. **18**, 698 (2024).

[19] J. Yan, W. Qin, Y. Chen, W. Decking, P. Dijkstal, M. Guetg, I. Inoue, N. Kujala, S. Liu, T. Long, N. Mirian, and G. Geloni, Terawatt-attosecond hard x-ray free-electron laser at high repetition rate, Nat. Photon. **18**, 1293 (2024).

[20] C. Emma, N. Majernik, K. K. Swanson, R. Ariniello, S. Gessner, R. Hessami, M. J. Hogan, A. Knetsch, K. A. Larsen, A. Marinelli, B. O'Shea, S. Perez, I. Rajkovic, R. Robles, D.

Storey, and G. Yocky, Experimental generation of extreme electron beams for advanced accelerator applications, Phys. Rev. Lett. **134**, 085001 (2025).

[21] P. Muggli, V. Yakimenko, M. Babzien, E. Kallos, and K. P. Kusche, Generation of trains of electron microbunches with adjustable subpicosecond spacing, Phys. Rev. Lett. **101**, 054801 (2008).

[22] S. Bielawski, C. Evain, T. Hara, M. Hosaka, M. Katoh, S. Kimura, A. Mochihashi, M. Shimada, C. Szwaj, T. Takahashi, and Y. Takashima, Tunable narrowband terahertz emission from mastered laser–electron beam interaction, Nat. Phys. **4**, 390 (2008).

[23] Y.-E. Sun, P. Piot, A. Johnson, A. H. Lumpkin, T. J. Maxwell, J. Ruan, and R. Thurman-Keup, Tunable subpicosecond electron-bunch-train generation using a transverse-to-longitudinal phase-space exchange technique, Phys. Rev. Lett. **105**, 234801 (2010).

[24] Y. Shen, X. Yang, G. L. Carr, Y. Hidaka, J. B. Murphy, and X. Wang, Tunable few-cycle and multicycle coherent terahertz radiation from relativistic electrons, Phys. Rev. Lett. **107**, 204801 (2011).

[25] P. Musumeci, R. K. Li, and A. Marinelli, Nonlinear longitudinal space charge oscillations in relativistic electron beams, Phys. Rev. Lett. **106**, 184801 (2011).

[26] S. Antipov, C. Jing, M. Fedurin, W. Gai, A. Kanareykin, K. Kusche, P. Schoessow, V. Yakimenko, and A. Zholents, Experimental observation of energy modulation in electron beams passing through terahertz dielectric wakefield structures, Phys. Rev. Lett. **108**, 144801 (2012).

[27] S. Antipov, M. Babzien, C. Jing, M. Fedurin, W. Gai, A. Kanareykin, K. Kusche, V. Yakimenko, and A. Zholents, Subpicosecond bunch train production for a tunable mJ level THz source, Phys. Rev. Lett. **111**, 134802 (2013).

[28] Z. Zhang, L. Yan, Y. Du, Z. Zhou, X. Su, L. Zheng, D. Wang, Q. Tian, W. Wang, J. Shi, H. Chen, W. Huang, W. Gai, and C. Tang, Tunable high-intensity electron bunch train production based on nonlinear longitudinal space charge oscillation, Phys. Rev. Lett. **116**, 184801 (2016).

[29] F. Lemery, P. Piot, G. Amatuni, P. Boonpornprasert, Y. Chen, J. Good, B. Grigoryan, M. Groß, M. Krasilinikov, O. Lishilin, G. Loisch, A. Oppelt, S. Philipp, H. Qian, Y. Renier, F. Stephan, and I. Zagorodnov, Passive ballistic microbunching of nonultrarelativistic electron bunches using electromagnetic wakefields in dielectric-lined waveguides, Phys. Rev. Lett. **122**, 044801 (2019).

[30] G. Zhao, S. Zhao, S. Huang, and K. Liu, Strong electron density modulation with a low-power THz source for generating THz superradiant undulator radiation, Phys. Rev. Accel. Beams **22**, 060701 (2019).

[31] H. Feng, Z. Zhou, Y. Wu, Z. Gao, Y. Liang, N. Huang, L. Yan, H. Deng, Y. Du, R. Li, W. Lu, W. Huang, and C. Tang, Generation of tunable 10-mJ-level terahertz pulses through nonlinear plasma wakefield modulation, Phys. Rev. Appl. **15**, 044032 (2021).

[32] Y. Liang, Z. Liu, Q. Tian, T. Li, X. Lin, L. Yan, Y. Du, R. Li, J. Shi, C. Cheng, W. Huang, and C. Tang, Widely tunable electron bunch trains for the generation of high-power narrowband 1–10 THz radiation, Nat. Photon. **17**, 259 (2023).

[33] T. Tanaka, Proposal to generate an isolated monocycle X-ray pulse by counteracting the slippage effect in free-electron lasers, Phys. Rev. Lett. **114**, 044801 (2015).

[34] V. A. Goryashko, Quasi-half-cycle pulses of light from a tapered undulator, Phys. Rev. Accel. Beams **20**, 080703 (2017).

[35] H. Zhang, W. Wang, S. Jiang, C. Li, Z. He, Q. Jia, L. Wang, and D. He, Generation of frequency-chirped density modulation electron beam for producing ultrashort THz radiation pulse, Phys. Rev. Accel. Beams **23**, 020704 (2020).

[36] S. Ma, H. Zhang, J. Pang, C. Liu, and Z. He, Enhancement of chirped density modulation in electron beam for generating ultrashort THz radiation pulse, Phys. Rev. Accel. Beams **28**, 044402 (2025).

[37] X. Li, Y. Yu, Q. Li, S. Liu, C. Wang, J. Zhou, F. Yin, X. Shi, J. Sun, J. Shao, X. Wang, Z. He, W. Dong, L. Jiang, J. Yang, G. Wu, W. Zhang, and X. Yang, Wavelength switching and scanning of the high-gain harmonic generation free-electron laser at the Dalian Coherent Light Source, Phys. Rev. Accel. Beams **28**, 100701 (2025).

[38] DESY mpyflo, https://www.desy.de/mpyflo/, accessed 6 June (2025).

[39] T. Tanaka and H. Kitamura, *SPECTRA*: A synchrotron radiation calculation code, J. Synchrotron Rad. **8**, 1221 (2001).

[40] A. Murokh, J. Rosenzweig, M. Hogan, H. Suk, G. Travish, and U. Happek, Bunch length measurement of picosecond electron beams from a photoinjector using coherent transition radiation, Nucl. Instrum. Methods Phys. Res. Sec. A **410**, 452 (1998).

[41] M. Castellano, V. A. Verzilov, L. Catani, A. Cianchi, G. Orlandi, and M. Geitz, Measurements of coherent diffraction radiation and its application for bunch length diagnostics in particle accelerators, Phys. Rev. E **63**, 056501 (2001).

[42] https://cstr.cn/31127.02.dcls.